Elasticity of Plagioclase Feldspars

J. Michael Brown
Department of Earth and Space Sciences
Box 35-1310
University of Washington
Seattle, WA 98195
brown@ess.washington.edu

Ross J. Angel*
Virginia Tech Crystallography Laboratory
Department of Geosciences
Virginia Tech
Blacksburg VA 24060-0420 USA

Nancy Ross
Virginia Tech Crystallography Laboratory
Department of Geosciences
Virginia Tech
Blacksburg VA 24060-0420 USA

*Now at: Department of Geosciences, University of Padova, Via G. Gradenigo 6, I-35131 Padova, Italy.

Abstract:

Elastic properties are reported for seven plagioclase feldspars that span compositions from albite ($NaSi_3AlO_8$) to anorthite ($CaSi_2Al_2O_8$). Surface acoustic wave velocities measured using Impulsively Stimulated Light Scattering and compliance sums from high-pressure X-ray compression studies accurately determine all 21 components of the elasticity tensor for these triclinic minerals. The overall pattern of elasticity, and the changes in individual elastic components with composition can be rationalized on the basis of the evolution of crystal structures and chemistry across this solid-solution join. All plagioclase feldspars have high elastic anisotropy; *a** (the direction perpendicular to the *b*- and *c*-axes) is the softest direction by a factor of 3 in albite. From albite to anorthite the stiffness of this direction undergoes the greatest change, increasing two-fold. Small discontinuities in the elastic components, inferred at boundaries between the three structural phases ($C\bar{1}$, $I\bar{1}$, and $P\bar{1}$), appear consistent with the nature of the underlying conformation of the framework-linked tetrahedra and the associated structural changes. Body wave velocities measured plagioclase-rich rocks, reported over the last five decades, are consistent with calculated Hill-averaged velocities using the current moduli. This confirms longstanding speculation that previously reported elastic moduli for plagioclase feldspars are systematically in error. The current results provide greater assurance that the seismic structure of the mid and lower crust can be accurately estimated on the basis of specified mineral modes, chemistry, and fabric.

Index Terms: 3620 3909 3924 7205 7220

1. Introduction

Knowledge of the complete elastic properties of the constituent minerals of rocks is a prerequisite for predicting and interpreting the seismic response of Earth's crust. Plagioclase feldspars are a dominant mineral group in both the continental and oceanic crust. Both their isotropic and the anisotropic elastic responses, associated with mineral fabric or (lattice) preferred orientations (the so-called LPO) are needed for the range of naturally occurring compositions, at temperatures and pressures appropriate for the crust. However, because they have triclinic symmetry, 21 individual elastic moduli are necessary to describe their single crystal properties and, as a consequence, their full elastic tensors have never been previously determined except for one end-member [*Brown et al.*, 2006]. Here, all moduli at one bar are reported for seven samples that span plagioclase compositions.

Plagioclase feldspars found in crustal rocks have major element compositions that fall along the anorthite ($CaAl_2Si_2O_8$) – albite ($NaAlSi_3O_8$) join (given here as the anorthite content, An_x with x ranging from 0 to 100), with the exchange of Ca^{2+} for Na^+ coupled to a change in the Al,Si ratio. The chemistry and phases of crustal feldspars is further discussed in the Auxiliary Materials. All feldspars have a fully polymerized three-dimensional framework of AlO_4 and SiO_4 tetrahedra. The framework is built up from rings of four tetrahedra that lie approximately perpendicular to the *b*-axis (Figure 1a). These 4-rings are linked to form the "crankshaft" [*Megaw,* 1970] chains that extend along the *a*-axis and are characteristic of the feldspar structure type (Figure 1b). Sheets of chains are further linked together along the *b*-axis to form the cavities for the extra-framework cations, Na^+ and Ca^{2+} (Figure 1c). Despite the three-dimensional connectivity of the tetrahedral framework of feldspars, compression measurements [e.g. *Angel et al*., 1988; *Benusa et al.,* 2005], and determinations of the elastic tensor [*Brown et al.,* 2006] have shown that all feldspars, irrespective of either framework composition or the extra-framework cation, are as elastically anisotropic as sheet silicates. This anisotropy arises from the topology of the framework. The "crankshaft" chains (Figure 1b) can be closed up or extended relatively easily (e.g. *Smith and Brown*, [1988] page 55) because this can be accomplished by cooperative rotations of effectively rigid tetrahedra without any deformations of the tetrahedra [*Angel et al.,* 2012; 2013]. As a consequence, changes in the distribution of Al,Si between the tetrahedral sites has only a small effect on the bulk moduli of plagioclase feldspars [*Sochalski-Kolbus et al.,* 2010].

Efforts to connect the seismic response of Earth's interior to the elasticity of its constituents have involved high-pressure laboratory studies [*e.g. Christensen and Mooney,* 1995]). In the case of plagioclase-rich rocks, the compositional dependence of compressional wave velocities to 1 GPa was reported by *Birch* [1961]; additional data at high pressure on essentially mono-mineralic aggregates (including determinations of shear wave velocities) are reported in [*Simmons*, 1964; *Liebermann and Ringwood,* 1976; *Seront et al.,* 1993; *Mueller et al*., 2002]. Application of pressures greater than 0.2-0.5 GPa is typically assumed sufficient to adequately close cracks so that measured velocities are representative of the intrinsic mineral elasticity. However, low aspect ratio cracks may not close under such pressures and velocities may remain systematically below intrinsic values.

Prior measurements of the compressibility of the feldspars (the response to hydrostatic pressure) (*e.g. Angel* [2004]) are not sufficient to fully determine the elastic modulus or compliance tensors. Thus, the only primary source of data for the full elastic properties of plagioclase feldspar crystals as a function of composition is the pioneering one-bar ultrasonic measurements of twinned megacrysts by *Ryzhova* [1964], and this work has been extensively cited. Unfortunately, as documented in *Brown et al.* [2006], the data acquisition scheme used by *Ryzhova* [1964], could not adequately determine all 13 elastic tensor components in the pseudo-monoclinic samples, nor the values of the additional 8 components that are allowed in crystals with triclinic symmetry.

The elastic properties of a mineral aggregate in which the cracks are fully closed must fall between the Voigt (upper) and Reuss (lower) bounds that can be calculated from the single-crystal elastic moduli and compliances. [*Hill,* 1963]. In the absence of microstructure knowledge (e.g. *Mainprice et al.* [2011]), the Hashin-Shtrikman bounds provide the tightest possible estimates for aggregate behavior [*Watt et al.,* 1976]. Results in a number of studies [*Christensen*, 1966; *Liebermann and Ringwood*, 1976; *Seront et al.*, 1993; *Brown et al.*, 2006] have indicated that moduli reported by *Ryzhova* [1964] might be biased to low values, possibly as a result of the samples having open cracks. Alternatively, accepting *Ryzhova*'s result leads to a match between measured rock velocities and the calculated Voigt bound [*Seront et al.,* 1993]. For feldspar-rich rocks, this lies well above the Hashin-Shtrikman upper bound. This empirical correlation indicates that either the rock velocities are in error or that one of the other characteristics of the rock (either the texture or the elastic properties of the constituent phases) is in error.

The elastic moduli reported here are interpreted in terms of the underlying structural conformation, changes in composition, and the structural states of plagioclase minerals. These data provide an ideal opportunity for reassessing the interpretation of measured compressional and shear wave velocities in feldspar-rich rocks, and also for addressing more general issues of the elastic response of aggregates. The extreme elastic anisotropy of feldspars, with the Reuss and Voigt bounds on the shear modulus differing by 30% and the bulk moduli differing by 20% make them ideal for resolving the question as to whether or not rock properties fall close to the (Hill) average between the upper and lower bounds and within the tighter Hashin-Shtrikman bounds recommended by *Watt et al.* [1976].

2. Sample sources and characterization

The sources, chemistry, localities, and structural state of seven samples are given in Table S1 of the Auxiliary Materials. Together with the end-member albite [*Brown et al.,* 2006], the six additional samples measured in this study were chosen so as to cover the compositional range of plagioclase feldspars and to represent the variety of structural states ($C\bar{1}$, $I\bar{1}$, and $P\bar{1}$) most commonly found in natural plagioclases. Changes in the patterns of Al,Si order within the tetrahedra result in symmetry changes that can be identified by changes in the diffraction patterns [*Bown and Gay*, 1958; *Angel et al.,* 1990]. The degree of Al,Si order can be determined from the tetrahedral bond lengths determined by structure refinements [*Ribbe*, 1983; *Kroll and Ribbe* 1983; *Salje,* 1985]. The change in the Al,Si ratio away from a simple integer ratio means that some Al,Si disorder is induced by the chemical substitution away from the end-member compositions of albite and anorthite. Single-crystal X-ray diffraction data were therefore collected from one crystal from each sample on a variety of Oxford Diffraction CCD diffractometers. Full details of the data collections, structure refinements and final refined structural parameters are reported in the Auxiliary Materials crystallographic information file *(cif)*. In summary, six of the samples are well ordered and are thus “low plagioclases” with thermodynamic and elastic properties typical of plagioclases in crustal rocks. An_{60} is a relatively disordered “high-plagioclase” [*Kroll and Ribbe*, 1980] on the basis of its unit-cell parameters and refined structure. TEM observations of the An_{48} sample confirmed that it is a Bøggild intergrowth, a composite crystal containing coherent lamellae of approximate compositions An_{45} (symmetry $C\bar{1}$) and An_{55} (symmetry $I\bar{1}$). In Table 1 cell parameters, unit cell volumes, and densities (calculated from the chemistry and cell volumes) are given for the samples.

Following *Brown et al.* [2006], we chose the following convention to align the non-orthogonal crystallographic axes with respect to the Cartesian axial system used for the description of the elastic tensor. The Y-axis is aligned parallel to the crystallographic *b*-axis. The X-axis is set in the *a** direction (perpendicular to the *b*- and *c*-axes). The Z-axis is chosen to satisfy a right-handed coordinate system. This convention is different from that used by *Ryzhova* [1964] who also set the Y-axis parallel to the *b*-axis, but then set the Z-axis parallel to *c**. Relative to our system, these coordinates are rotated ~26° about the *b*-axis. Although *Ryzhova's* convention was motivated by the nature of the underlying crystal structure (placing the extension direction of the crankshaft chain within the structures of plagioclase feldspars parallel to the X-axis) it results in compressional velocities in the X-Z plane that enjoy no simple relationship to the Cartesian coordinates. With the convention used here, maxima and minima of the compressional velocities lie closer to the coordinate axes, with the extreme values determined principally by a single elastic modulus. We use the convention that the elastic moduli (stiffnesses) are represented by the 6 by 6 matrix $\boldsymbol{C_{ij}}$. The inverse of this matrix is the compliance matrix $\boldsymbol{S_{ij}}$. These matrixes are related to the full tensor representation of elasticity by the Voigt notation [*Nye*, 1957].

3. Experimental methods:

3.1 X-ray Compressibility Determinations:

Adding to measurements previously reported [*Angel*, 2004], the unit-cell compressions of the An_{48}, An_{60}, and An_{96} samples used in this study were measured in diamond-anvil cells by single-crystal diffraction using a Huber 4-circle diffractometer [*Angel et al.,* 1997] run by the Single software [*Angel & Finger*, 2011]. Pressures were determined from the measured unit-cell volume of a quartz crystal included in the cell with each sample and its equation-of-state [*Angel et al.,* 1997]. Unit cell data for the other plagioclase compositions were taken from *Angel* [2004]. Values of the components of the compressibility matrix $\beta_i = \boldsymbol{S}_{i1} + \boldsymbol{S}_{i2} + \boldsymbol{S}_{i3}$ at room pressure were determined in two ways. For the three elements corresponding to normal strains (*i* = 1-3), Birch-Murnaghan equations of state were fit to the variations with pressure of the cubes of the unit-cell dimensions corresponding to the X, Y, and Z Cartesian axial directions to obtain the room-pressure values of compressibility. This approach cannot be applied to the shear elements of the compressibility matrix (i = 4-6). Therefore for both these and the normal strains, the components of the incremental Eulerian finite strain ε_i were calculated from the unit-cell parameters of each pair of consecutive data points to yield the compliance tensor component sums $\beta_i = -\varepsilon_i/\Delta P$, in which ΔP is the pressure increment between data points. Plots of each of the 6 compliance sums against the average pressure of the pair of data points were then extrapolated back to zero to provide a constraint on the room pressure values of the compressibility matrix elements for each crystal. For the normal compressibilities (β_i, i = 1-3) the two methods yielded the same values within the estimated uncertainties (Figure 2). Their variation with composition across the $C\bar{1}$ and $I\bar{1}+P\bar{1}$ phases (*i.e.* for An_0- An_{50} and for An_{50}-An_{100} separately) was then fitted with appropriate polynomials as shown in Figure 2. An additional distinction was made between the $I\bar{1}$ and $P\bar{1}$ phases for β_5 and β_6. The values from these fits were then used as constraints in the subsequent analysis to determine the full set of elastic parameters from the measured wave velocities.

3.2 Acoustic Velocity and Elastic Parameters Determinations:

Surface acoustic wave (SAW) velocities were measured using the method of Impulsive Stimulated Light Scattering (ISLS) [*Abramson et al.,* 1999]. Details of the experiment and the method to determine elastic parameters for triclinic feldspars are described in *Brown et al.* [2006]. New in this work was the use of the “Trust Region Interior Reflective Method” [*Coleman and Li,* 1994, 1996] to find an optimal set of elastic moduli that best fit measured surface-wave velocities and the compressibilities (Figure 2) determined in the high-pressure X-ray measurements. A “multi-start” approach was adopted in which optimization is initiated many times from sets of elastic moduli that are randomly generated in the range of an *a priori* “trust region” (set to insure that the elasticity tensor remains positive definite). The best solution is identified and, within the stated uncertainties, is thought to be unique for each data set. A Monte Carlo analysis provided support for this conjecture. Synthetic data with random errors and propagation coverage comparable to the actual data were generated from known sets of elastic moduli. The inversion method used here recovered the *a priori* moduli within the estimated uncertainties.

Elastic moduli $\boldsymbol{C_{ij}}$ and their associated 2σ uncertainties for all plagioclase samples are listed in Table 2. The first nine moduli in each column are those allowed to be non-zero under orthorhombic symmetry ($\boldsymbol{C_{11}}$ $\boldsymbol{C_{22}}$ $\boldsymbol{C_{33}}$ $\boldsymbol{C_{44}}$ $\boldsymbol{C_{55}}$ $\boldsymbol{C_{66}}$ $\boldsymbol{C_{12}}$ $\boldsymbol{C_{13}}$ $\boldsymbol{C_{23}}$). The next four ($\boldsymbol{C_{15}}$ $\boldsymbol{C_{25}}$ $\boldsymbol{C_{35}}$ $\boldsymbol{C_{46}}$), in addition to the first nine, are allowed to be non-zero for monoclinic symmetry. Compliances ($\boldsymbol{S_{ij}}$) are listed in Table S2 of the Auxiliary Materials. Note that individual compliances are *not* the simple inverse of the modulus component with the same indices [*Nye*, 1957]. The values reported here for albite differ slightly from those in *Brown et al.* [2006] as a result of refitting the original velocity data with modified estimates for the uncertainties of the X-ray compliance sums. We have adopted a uniform uncertainty of 0.0001 GPa^{-1} for all of the compliance sums derived from the high-pressure X-ray measurements. This value is a conservative global estimate that exceeds both the formal fitting error, the data scatter of individual high-pressure data points, the spread in values determined by different methods of data reduction (section 3.1), and is the maximum misfit of smoothed trend lines fit through the data as a function of composition. Magnitudes of uncertainties for components $\boldsymbol{C_{11}}$, $\boldsymbol{C_{22}}$, $\boldsymbol{C_{33}}$, $\boldsymbol{C_{12}}$, $\boldsymbol{C_{13}}$, and $\boldsymbol{C_{23}}$ scale with uncertainties in X-ray compressibilities. Other moduli/compliances are fully constrained by the SAW data and their values and uncertainties are not impacted by the X-ray data. The 2σ uncertainties listed in the table were calculated from the covariance matrix [*Brown et al.* 1989] that included uncertainties in both the velocities (set to be 0.3%) and the X-ray determined compressibilities. Table S3 of the Supplementary Materials contains X-ray compliance determinations, all measured and predicted SAW velocities, and optimization results.

4. Discussion

4.1 Elastic Moduli, Compliances, and Body Wave Velocities

The elastic moduli and compliances are plotted in Figure 3 as a function of composition. Boundaries between the three symmetrically distinct phases of plagioclase ($C\bar{1}$, $I\bar{1}$, $P\bar{1}$) are also indicated. Within the range of composition of each phase, the data are linked by low order curves to guide the eye; most points lie within estimated uncertainty of these curves. Although a few components exhibit linear or mildly non-linear trends over the entire range of composition (for example $\boldsymbol{C_{11}}$ and $\boldsymbol{S_{11}}$), the majority of components cannot be adequately represented over the entire compositional range with a single low-order polynomial. Additional compositional data are needed to fully constrain behavior across the phase boundaries. Nevertheless, several components appear to have discontinuities larger than experimental uncertainties.

The orthorhombic elastic moduli (upper two rows of Figure 3) are larger (with the exception of $\boldsymbol{C_{23}}$ which is discussed below) and have smaller percentage changes with composition than the remainder of the off-diagonal components. However, as shown below, the non-orthorhombic components have non-negligible effects on calculated body wave velocities.

For diagonal matrix elements *ii* with i = 1-3, the most compliant direction is parallel to a^* (since X is set parallel to a^*, $\boldsymbol{C_{11}}$ is small and $\boldsymbol{S_{11}}$ is large). With increasing substitution of Ca^{2+} for Na^{1+} (and the coupled substitution of Al^{3+} for Si^{4+}), $\boldsymbol{C_{11}}$ stiffens significantly. The trend for $\boldsymbol{C_{11}}$ from albite to anorthite is essentially linear while $\boldsymbol{S_{11}}$ has distinctly nonlinear behavior; small discontinuities at the phase boundaries shown by the curves are comparable to the uncertainties. The other two longitudinal moduli and compliances associated with the Y and Z axes ($\boldsymbol{C_{22}}$/$\boldsymbol{S_{22}}$ and $\boldsymbol{C_{33}}$/$\boldsymbol{S_{33}}$) are nearly identical at An_0 and diverge slightly for An_{100}. $\boldsymbol{C_{22}}$/$\boldsymbol{S_{22}}$ appear to have discontinuities at the $C\bar{1}$ to $I\bar{1}$ transition that are larger than uncertainties. Although a continuous curve might be constructed through the $\boldsymbol{C_{33}}$ and $\boldsymbol{S_{33}}$ compositional trends, discontinuous segments are shown in the figure. The overall strong anisotropy of the elastic properties of albite and the decrease in anisotropy with increasing anorthite content is also reflected in the anisotropy of the thermal expansion coefficients [*Tribaudino et al.*, 2011] and must therefore reflect the fundamental anisotropy of the response of the three-dimensional tetrahedral framework of the feldspar structure to applied stresses and strains.

The diagonal shear components (matrix elements *ii* with i = 4-6, top rows, middle panels) relate applied shear strains with stresses having the same sense of shear direction. These components are well constrained by the SAW data as evidenced by the small experimental uncertainty. That low degree polynomial curves do not fit data within uncertainty in the $C\bar{1}$ range of composition may be a result of including the An_{48} sample. Since this crystal is a Bøggild intergrowth with lamellae of both $C\bar{1}$ and $I\bar{1}$ phases, elastic behavior intermediate between the two phases might be expected. $\boldsymbol{C_{44}}$ and $\boldsymbol{C_{66}}$ change little across the entire compositional series while $\boldsymbol{C_{55}}$ shifts from being nearly equal to $\boldsymbol{C_{44}}$ for albite to being nearly equal to $\boldsymbol{C_{66}}$ for anorthite. This change occurs entirely within the $C\bar{1}$ range of composition.

The off-diagonal longitudinal moduli and compliances (matrix elements 12, 13, and 23) relate compressive stresses to compressive strains in orthogonal directions. $\boldsymbol{C_{12}}$ and $\boldsymbol{C_{13}}$ are nearly equal and both double in the range from albite (~30 GPa) to anorthite (~60 GPa). The compliances, $\boldsymbol{S_{12}}$ and $\boldsymbol{S_{13}}$ are appropriately negative; a compressive stress along the X-axis generates an expansion in the orthogonal directions (Y and Z axes). However, the $\boldsymbol{C_{23}}$ modulus is anomalously small for albite and increases with anorthite content. A small value for $\boldsymbol{C_{23}}$ means that application of normal strain in just the Y direction results in a small normal stress in the Z direction. That $\boldsymbol{S_{23}}$ is positive for the $C\bar{1}$ plagioclases is unusual in that this indicates that a compressive stress along the Y axis gives rise to *contraction* along the Z-axis. Coesite also exhibits the same behavior [*Weidner and Carleton*, 1977] and has a similar, but not identical, tetrahedral framework to the feldspars. The structures of both minerals include 4-rings of tetrahedra that can undergo a torsional tilt that does not distort the tetrahedra (Figure 1a) [*Angel et al.,* 2003, 2012]. Simulations of the whole framework of feldspar show that the connectivity between these rings results in the torsion of all rings shortening the Y and Z directions simultaneously but leads to large expansion of the X direction (Figure 6 in [*Angel et al.,* 2012]). Thus the negative values of $\boldsymbol{S_{12}}$ and $\boldsymbol{S_{13}}$ and the positive value of $\boldsymbol{S_{23}}$ for $C\bar{1}$ plagioclases indicates that the elastic response of feldspars to individual normal stresses is, like their response to hydrostatic stress, accommodated by the mutual rotation of effectively rigid tetrahedra. Further modeling of the monoclinic feldspars [*Angel et al.,* 2013] shows that while distortions and changes in relative size of the tetrahedra (e.g. due to changes in Al,Si ordering) do not affect the overall pattern of anisotropy of the structure, they do generate changes in the unit-cell parameters and can modify the anisotropy by a few percent. Therefore it is not surprising that the weak co-variation of the *b*- and *c*-axes with the torsional tilt, which leads to the positive value of $\boldsymbol{S_{23}}$ for $C\bar{1}$ plagioclases is further weakened as the pattern of Al,Si order changes to that of the $I\bar{1}$ and $P\bar{1}$ phases and $\boldsymbol{S_{23}}$ becomes zero within uncertainty: a compressive stress along Y causes no strain in the Z direction.

The scales and limits of the ordinates are held constant to facilitate comparisons of the remaining (non-orthorhombic) elastic elements in Figure 3 (bottom two rows). All of these parameters are well determined solely on the basis of the surface wave velocity measurements. The discontinuities between the $C\bar{1}$, $I\bar{1}$, and $P\bar{1}$ phases shown in these figures provide additional support for the divisions adapted in interpreting the X-ray compliance sums as shown in Figure

2. The three panels on the left give moduli and compliances associated with the mapping of compressive stresses to shear strains (matrix elements *ij* with *i=1-3* and *j=4-6*). The far right panels gives the mapping between shear stresses and resulting shear strains in orthogonal directions. Most of the $\boldsymbol{S_{ij}}$ are small, ranging from -4 to +4 TPa^{-1} and the trends for individual elastic elements within each phase are complex and varied. Further, with the exception of $\boldsymbol{S_{46}}$, the values of the elements allowed under the aristotype monoclinic symmetry of feldspars (i.e. $\boldsymbol{S_{15}}$, $\boldsymbol{S_{25}}$, $\boldsymbol{S_{35}}$ and $\boldsymbol{S_{46}}$) are no larger than those elements whose values would be zero in monoclinic feldspars. However, the smaller discontinuities associated with the $C\bar{1}$ to $I\bar{1}$ transition in the values of the 'monoclinic' elements $\boldsymbol{S_{i5}}$ relative to those for the 'triclinic' elements $\boldsymbol{S_{i4}}$ and $\boldsymbol{S_{i6}}$ indicate that the elastic response of the plagioclases is still dominated by the response of the tetrahedral framework. This is supported, as we discuss below, by the observation that the $\boldsymbol{C_{ij}}$ with *j*=6 have generally larger discontinuities than those with *j*=4-5. This means that the change in shear stiffness of the X-Y plane (*j*=6) from $C\bar{1}$ to $I\bar{1}$ is larger than that of the perpendicular planes X-Z and Y-Z (*j*=4-5). Ignoring the cell-doubling along the *c-axis* that arises from the change in Al/Si ordering pattern, the transition results in small changes in the α and β unit-cell angles but a significant increase in the γ angle from ~90^{o} for $C\bar{1}$ plagioclases to ~91.5^{o} for $I\bar{1}$ plagioclases. Thus, the biggest change in the shear elastic moduli between $C\bar{1}$ and $I\bar{1}$ phases corresponds to the biggest difference between their unit-cell parameters.

Compressional and shear velocities in single crystals with respect to propagation directions relative to crystal axes are shown in Figure 4. For purely orthorhombic symmetry, velocities would exhibit mirror symmetry about the Cartesian coordinate axes. Although these triclinic velocities exhibit orthorhombic trends (*e.g.* the maximum and minimum compressional velocities lie close to the Cartesian axes), perturbations associated with the lower symmetry of the feldspar structure are clearly evident. Strong anisotropy of compressional velocities is observed in the X-Y and X-Z planes with the low velocities (<6 km/s) in the X direction (*a** crystallographic direction) and velocities exceeding 8 km/s along Y and Z. Shear wave velocities show strong anisotropy in the Y-Z plane; the highest shear velocities and greatest polarization dependence occur near the bisector of the *b-* and *c-* axes. At these points, the velocity of the fastest shear wave approaches the compressional wave velocity. With increasing anorthite content, compressional and shear velocities become less anisotropic (as indicated by more circular velocity trends).

4.2 Elasticity and structure

The overall pattern of elasticity variation and the resultant variation in compressibility elements across the plagioclase join (as shown in Figures 2-4) reflects the evolution of the structures of these feldspars. The dominant change in the framework conformation across the whole join is the reduction in the values of the same tetrahedral tilts (#2 and #3 in the notation of [*Megaw*, 1970; *Angel et al.,* 2012]) that follow exactly the same trend as found in alkali feldspars [*Angel et al.,* 2012, 2013]. This results from maximizing the length of the shortest O-O distances in the structure as the volume of the structure is changed [*Angel et al.,* 2012, 2013]. In the plagioclase feldspars, the relative values of the diagonal compressional moduli $\boldsymbol{C_{ii}}$ and compliances $\boldsymbol{S_{ii}}$ and the first three compressibilities β_i (i=1-3) can be explained in terms of these same tilts. The X direction is soft because the coupled changes in tilts 2 and 3 results in large strains in this direction, without changes in the short O-O distances (see Fig 8 in *Angel et al*. [2012]). The Y and Z directions are about 3 times stiffer than X under both hydrostatic compression (as represented by elements β_2 and β_3 in Figure 2) and normal stress ($\boldsymbol{S_{22}}$ and $\boldsymbol{S_{33}}$ in Figure 3) because the combination of tilts 2 and 3 does not produce large strains in these directions. The values, and the unusual positive sign of $\boldsymbol{S_{23}}$, of the off-diagonal compliances $\boldsymbol{S_{ij}}$ (i,j=1-3, $i \neq j$) that define the normal strains in directions perpendicular to an applied normal stress can be explained by the same mechanism. Other mechanisms that might be available to accommodate stress applied to the structures will be stiffer because they either generate smaller strains and shorten O-O distances (tilts 1 and 4) or they involve deformation of the stiff tetrahedra. The overall decrease in anisotropy that is observed in the compressibility, and in the normal compliances $\boldsymbol{S_{ii}}$, on going from albite towards anorthite cannot be directly due to the substitution of Al for Si in the framework but must, in some way, be the result of the coupled substitution of the Na of the albite component by Ca of the anorthite component.

The different changes in various moduli, compliances and compressibilities between the $C\bar{1}$, $I\bar{1}$, and $P\bar{1}$ plagioclases are related to the magnitudes of the corresponding changes in structure. First, the changes in the normal compressibilities β_i and normal compliances $\boldsymbol{S_{ij}}$ ($i,j=1,3$) are relatively small compared to their values (Figures 3-5), confirming that the values of these elastic elements are controlled by the topology of the framework and not by its detailed conformation as represented by the values of tilts. Most of the other elastic properties (β_i, $\boldsymbol{S_{ij}}$, $\boldsymbol{C_{ij}}$; $i,j = 4$-6) show relatively small jumps in values at the phase transition from $C\bar{1}$ to $I\bar{1}$, but significant changes in slopes; this is consistent with the observation that the tilts of the framework of $I\bar{1}$ plagioclase evolve smoothly with composition away from those of $C\bar{1}$ plagioclase close to the transition. Note that even if the transition is thermodynamically continuous as indicated by the trends in structure, discontinuities are allowed in the elastic properties at the transition point (e.g. [*Carpenter & Salje* 1998]). Neither the structural data nor the one available set of elasticity data for the $P\bar{1}$ plagioclases is sufficient to identify trends in elasticity within that phase. Nonetheless, it is clear that the large jumps in the values of some individual compliances, especially $\boldsymbol{S_{i6}}$ which indicate significant changes in the shear stiffness of the X-Z plane, are related to the change in the pattern of the shears of the 4-rings of tetrahedra within the structure. Within $C\bar{1}$ structures there is only one type of ring, so each layer of tetrahedral rings in the X-Z plane contains rings all sheared in the same sense, while consecutive X-Z layers are sheared in the opposite sense. Naïve mechanical considerations would suggest that stiffness of the structure in response to shear in the X-Z plane would be significantly different when the layers contain rings sheared in opposite senses (as in $I\bar{1}$ structures) and when the rings are sheared by far greater angles of more than 10^{o} in both senses in $P\bar{1}$ anorthites.

In summary, the measured patterns of compressibilities (response to hydrostatic stress) and of compliances and moduli (response to individual stresses and strains) for plagioclase feldspars are not just internally consistent. They are also consistent with what is known about the structures and the changes in structures with composition and between the three symmetrically distinct phases. However, it is important to note that, while we can relate all of the changes in elasticity to changes in structural conformations, it is not possible to determine whether these changes are the direct influence of stronger bonds for Ca relative to Na interacting with framework oxygen atoms, or a consequence of shorter O-O distances as the Ca content is increased and the conformation of the framework, as quantified by tetrahedral tilts, changes.

4.3 Applications to Aggregate Elasticity

4.3.1 Isotropic Average Bulk and Shear Moduli:

Isotropic estimates for the bulk and shear moduli, the Voigt, Reuss, Hill, (V-R-H) and Hashin-Shtrikman (H-S) bounds [*Brown* 2013] of the seven samples are listed in Table S3 of the Auxilary Materials. In Figure 5 (left side) these isotropic parameters are plotted as a function of composition. Experimental uncertainties for individual moduli are appropriately propagated and are shown with error bars given only for the Hill average.

The X-ray diffraction measurements were performed under uniform stress (hydrostatic compression) and so yield an isothermal bulk modulus that is equal to the Reuss bound (as shown in Figure 5). The conversion factor between the adiabatic and isothermal bulk moduli is (1+αγT). For plagioclase, the room-temperature volume thermal expansion coefficient α ranges from 2.89 x 10^{-5} K^{-1} for albite to 1.53 x 10^{-5} K^{-1} for anorthite [*Tribaudino et al.*, 2010], while the Grüneisen parameter γ remains approximately constant at 0.45±0.05 [*Tribaudino et al.*, 2011]. The ratio between the isothermal and adiabatic bulk moduli of plagioclase thus ranges from 0.4% to 0.2%, and is therefore smaller than the experimental uncertainties and is neglected.

The bulk modulus has a strong compositional dependence that is associated with the increasing stiffness along the $a*$ direction. In detail, the small offset at the $C\bar{1}$ to $I\bar{1}$ phase boundary noted by *Angel* [2004] is supported by the new data. In contrast, the shear modulus is relatively insensitive to composition. The Voigt bound is essentially independent of composition, while the Reuss bound has a slight positive slope. Albite is unusually anisotropic and anorthite, while still strongly anisotropic, has significantly narrower V-R bounds. The H-S bounds are consistently narrower than the V-R bounds. The Hill averages consistently lie within the H-S bounds for all compositions studied.

4.3.2 Isotropic and Anisotropic Anorthosite Velocities

In Figure 5 middle panels, one-bar rock velocities corrected from 1 GPa measurements (these are small correction; see Table S4 and notes in Auxiliary Materials) are compared with velocities calculated using the current isotropic moduli. Nominal uncertainties of 1% (compressional) and 2% (shear) are shown for reference. The trends in rock velocities with composition are well predicted by the current moduli. Compressional velocities increase from about 6.4 km/s for albite to about 7.2 km/s for anorthite. Shear wave velocities change by about 0.1 km/s. A detailed comparison of data with the calculated bounds is difficult in the face of experimental scatter and limited documentation. The Voigt-Reuss bounds are particularly wide for feldspars. Although the H-S bounds provide better constraints (narrowed bounds), nearly all rock velocities agree within uncertainty (grey bands) with the simple average of the V-R bounds, the Hill average. Distinguishing between H-S bounds and the Hill estimate will require rock velocity measurements with significantly smaller uncertainties. However, the current work demonstrates that a correct description of intrinsic mineral elasticity allows calculation of aggregate properties that agree within mutual uncertainties with measurement.

Deformed rocks containing plagioclase feldspars frequently exhibit LPO with a strong alignment of the *b*-axes and girdles of *a*- and *c*-axes [*Xie et al.* 2003]. Such a fabric leads to pseudo-hexagonal symmetry (transverse anisotropy) that requires just five elastic moduli to describe. In the work of *Seront et al.* [1993] on an anorthosite of An_{68} composition with about 10% by volume olivine, the orientations of plagioclase crystals within the rock were determined and velocities were measured at high pressure in specified directions with controlled polarizations relative to the measured LPO. Their rock had highly (but not perfectly) aligned plagioclase *b*-axes with equatorial girdles of *a*- and *c*-axes. The olivine had a distinctly different LPO. Velocities at 0.8 GPa were taken to represent the crack-free intrinsic response of the constituent minerals. They found that velocities based on their measured fabric best matched the Voigt average calculated from the elastic data of *Ryzhova* [1964]. As noted above, this suggests a fundamental problem with either the elastic moduli or the measurements on the rock sample.

We re-estimate properties for the anorthosite of *Seront et al.* [1993] using elastic moduli based on the current measurements. A large set of about 4000 crystal orientations that share the statistical properties similar to those measured in the rock were generated. The combination of a variance of 25° from complete alignment of *b*-axes and a randomization of the orientations of the *a*- and *c*-axes relative to the symmetry axis generates pole figures that visually match the distributions shown in Figure 5 of *Seront et al.* Since we found by calculation that the degree of LPO of the minority phase (olivine) has nearly negligible impact on the overall anisotropy of the rock, isotropic one-bar values from *Abramson et al.* [1997] are used in the results given here. The elastic moduli for the ensemble of 3600 An_{68} (moduli interpolated from our measurements) and 360 Fo_{89} crystals were averaged to determine aggregate Voigt, Reuss, and Hill bounds. Velocities were calculated as a function of angle from the transverse anisotropy axis. Based on the pressure dependence for isotropic compressional wave velocities (small) and shear wave velocities (nearly negligible), an isotropic correction of 0.08 km/s was added to calculated compressional velocities. Shear velocities of plagioclase in this compositional and pressure range are presumed to have essentially no pressure dependence.

Velocities as a function of angle relative to the transverse axis as reported in *Seront et al.* [1993] and those predicted using the current Hill-averaged elastic moduli are shown on the right side in Figure 5. Measured velocities along the *b*-axis cluster (the hexagonal symmetry axis) and in the symmetry plane (equatorial girdle) are reasonably matched by the predictions. The deviations between prediction and measurement found in the intermediate directions trend to velocities slightly below the prediction. A distribution of low aspect cracks that were not fully closed at the highest pressures may contribute to the velocities bias. However, general trends of velocities with direction are appropriately matched. Measured shear wave velocities in the intermediate directions, although biased low relative to the predictions, show appropriate polarization-dependent splitting. In contrast to the findings of *Seront et al.* who used elastic moduli based on results of *Ryzhova* [1964] the current Hill-averaged elastic moduli give an adequate accounting of the rock properties, and thus the non-physical situation represented by the previous match to Voigt moduli (Figure 16 in [*Seront* et al., 1993]) is resolved. The bias (about 0.1-0.2 km/s) in intermediate directions of the measured compressional and shear velocities may include a contribution associated with a distribution of crystal orientations that was not, in detail, perfectly transversely anisotropic; the isovelocity contours (Figures 11 and 12 in [*Seront* et al., 1993]) suggest deviations from pseudo-hexagonal symmetry.

The range of pressure in the crust (1 GPa in continental crust at a depth of 35 km) changes compressional velocities by ~ 0.1-0.2 km/s. Since the pressure-induced change of the shear modulus is almost cancelled by the increase in density, shear wave velocities are essentially pressure independent within the crust. Although the detailed temperature dependence of feldspar elastic properties remains to be determined, [*Christensen and Mooney*, 1995] suggest that intrinsic temperature effects within the crust are fairly small. *Christensen and Money* [1995] compared compressional velocities of common rocks with average crust and upper mantle seismic structure. Although the average anisotropy of feldspar-rich rock in their suite of samples was less than 10%, it is noteworthy that the compressional anisotropy in the anorthosite of *Seront et al.* [1993] is greater. A large body of anorthosite with a consistent LPO, as might be created in regional deformation events, could be interpreted as crustal (V_p<7.5) or mantle (V_p≈8 km/s) depending on its orientation in the crust relative to seismic wave propagation directions.

5. Conclusions

Elastic properties are reported for seven plagioclase feldspars that span the compositions from albite ($NaSi_3AlO_8$) to anorthite ($CaSi_2Al_2O_8$). Surface acoustic wave velocities measured using Impulsively Stimulated Light Scattering and compliance sums from high-pressure X-ray compression studies accurately determine all 21 components of the elasticity tensor for these triclinic minerals for the first time. The overall pattern of elasticity and compressibility can be explained in terms of the structural response of all feldspars to applied stress being dominated by the tilting of effectively rigid AlO_4 and SiO_4 tetrahedra that comprise the corner-linked framework of the crystal structure of feldspars. In particular, the flexibility of the framework results in strong anisotropy in both compressibilities and compliances, with the a^* direction in albite being softer by a factor of three than the perpendicular directions. The trends in the elasticity components can be rationalized on the basis of changes in crystal structure and chemistry across this solid-solution join. From albite to anorthite the stiffness in the a^* direction undergoes the greatest change, increasing two-fold, and represents the stiffening of the dominant mechanism of elastic response of the tetrahedral framework. Small discontinuities in the elastic components, inferred at boundaries between the three phases ($C\bar{1}$, $I\bar{1}$, and $P\bar{1}$), appear consistent with the nature of the underlying conformation of the framework-linked tetrahedra and the associated structural changes. Although Al,Si ordering is expected to have a relatively small impact on the elastic properties, ordering increases in both directions from the $C\bar{1}$ - $I\bar{1}$ transition and changes in slope at the boundary is probably an effect of the change in the pattern of ordering.

The current results provide greater assurance that the seismic structure of the mid and lower crust can be accurately estimated on the basis of specified mineral modes, chemistry, and fabric. Body wave velocities measured in nearly isotropic plagioclase-rich rocks, reported over the last five decades, are consistent with calculated Hill-averaged velocities using the current moduli. Velocities and their trends with composition are accurately predicted. This confirms longstanding speculation that previously reported elastic moduli for plagioclase feldspars are systematically in error. Velocities calculated using the new moduli document a high degree of anisotropy that moderately decreases with increasing anorthite content. Typical patterns of deformation-induced fabric (LPO) in feldspar-rich rocks lead to anisotropic velocities that can range from those typical for the lower crust to values associated with the upper mantle depending on the direction of seismic wave propagation relative to the fabric. Thus, variable chemistry and variable anisotropy can control the seismic structure of feldspar-rich crustal rocks.

Acknowledgments: This material is based upon work supported by the National Science Foundation through grant EAR-0711591 (JMB) and EAR-1118691 (NLR and RJA). The following undergraduate students contributed to this project: A. Teel, S. Pendleton, E. Chang, A. Pitts, H. West-Foyle, and K. Straughan. We thank S. Kuehner for microprobe analyses and W. Kaminsky for assistance in aligning crystals. We are grateful for E. Abramson's efforts in maintaining the ISLS laboratory and in solving experimental problems. High-pressure single-crystal diffraction data were collected at the Virginia Tech Crystallography Laboratory by Eleda Johnson. We thank Huifang Xu (Wisconsin) for the high-resolution TEM examination of the An_{48} sample. B. Evans (Seattle), R. Downs (Ariziona), J. Selverstone (Albuquerque), G. Rossman (CIT), M. Carpenter (Cambridge) and the National Musuem of Natural History at the Smithsonian Institution are thanked for the donation of samples for this project. We are grateful for discussions with Mario Tribaudino (Parma) and R. Liebermann (Stonybrook). R.L Carlson (TAMU) and N.I. Christensen (Wisconsin) are acknowledged for their long-standing inspirational enthusiasm for the subject.

References

Abramson, E. H., L. J. Slutsky, and J. M. Brown (1994), Elastic constants, interatomic forces and equation of state of β-oxygen at high pressure, *J. Chem, Phys.,* 100, 4518-4526.

Abramson, E. H., J. M. Brown, L. J. Slutsky, and J. Zaug (1997), The elastic constants of San Carlos olivine to 17 GPa, *J. Geophys. Res., 102*, 12,253-12,263.

Abramson, E. H., J. M. Brown, and L. J. Slutsky (1999), Applications of impulsive stimulated scattering in the earth and planetary sciences, *Ann. Rev. Phys. Chem., 50*, 279–313.

Angel R.J., R. M. Hazen, T. C. McCormick, C. T. Prewitt, J. R. Smyth (1988), Comparative compressibility of end-member feldspars. *Phys. Chem. Minerals*, **15**, 313-318.

Angel, R. J., M. A. Carpenter, and L. W. Finger (1990), Structural variation associated with compositional variation and order-disorder behavior in anorthite-rich feldspars, *Amer. Mineral.*, *75*(1-2), 150-162.

Angel, R. J., D. R. Allan, R. Miletich, and L. W. Finger (1997), The use of quartz as an internal pressure standard in high-pressure crystallography, *J. Appl. Cryst.*, *30*, 461-466.

Angel, R. J., C. S. J. Shaw, and G. V. Gibbs (2003), Compression mechanisms of coesite, *Phys. Chem. Minerals*, *30*, 167-176.

Angel, R.J. (2004), Equations of state of plagioclase feldspars, *Contrib. Mineral. Petrol. 146*, 506–512, doi:10.1007/s00410-003-0515-5.

Angel, R. J., J. M. Jackson, H. J. Reichmann, and S. Speziale (2009), Elasticity measurements on minerals: a review, *Eur. J. Mineral.*, *21*, 525-550.

Angel R.J., and L.W. Finger (2011): SINGLE: a program to control single-crystal diffractometers. *J. Appl. Cryst.*, **44**, 247-251.

Angel R.J., L.M. Sochalski-Kolbus, and M. Tribaudino (2012), Tilts and tetrahedra: the origin of anisotropy of feldspars. *Amer. Mineral.*, **97**, 765-778.

Angel R. J., N. L. Ross , J. Zhao, L. M. Sochalski-Kolbus, H. Krüger, and B. C. Schmidt (2013), Structural controls on the anisotropy of tetrahedral frameworks: the example of monoclinic feldspars. *Eur. J. Mineral.*, in press

Benusa, M., R. J. Angel, and N. L. Ross (2005), Compression of albite, $NaAlSi_3O_8$., *Amer. Mineral.*, *90*, 1115-1120.

Birch, F. (1961), The velocity of compressional waves in rocks to 10 kilobars, part 2*, J. Geophys. Res., 66*, 2199-2224.

Bown, M.G., and P. Gay (1958), The reciprocal lattice geometry of the plagioclase feldspar structures. *Z. Kristallogr. 111*, 1-14.

Brown, J. M., L. J. Slutsky, K.A. Nelson, and L-T. Cheng (1989), Single crystal elastic constants for San Carlos Peridot: An application of impulsive stimulated scattering, *J. Geophys. Res., 94,* 9485-9492.

Brown, J. M., E. H. Abramson, and R. J. Angel (2006), Triclinic elastic constants for low albite, *Phys. Chem. Minerals*, doi: 10.1007/s00269-006-0074-1.

Brown, J. M., Determination of Hashin-Shtrikman bounds on the effective elastic moduli of polycrystals of any Symmetry, Computers and Geosciences, submitted 2013.

Carpenter, M.A. (1986), Experimental delineation of the "e"= $I\bar{1}$ and "e" = $C\bar{1}$ transformations in intermediate plagioclase feldspars. *Phys. Chem. Minerals 13*,119-139.

Carpenter, M.A., J.D.C. McConnell, A. Navrotsky (1985), Enthalpies of ordering in the plagioclase feldspar solid solution. *Contribs. Min. Pet. 87*, 138-148.

Carpenter M.A., Salje E.K.H. (1998): Elastic anomalies in minerals due to structural phase transitions. *Eur. J. Mineral.*, **10**, 693-812.

Christensen, N. I. (1966), Compressional wave velocities in single crystals of alkali feldspar at pressures to 10 kilobars, *J. Geophys. Res., 71*, 3113-3116.

Christensen, N. I., W. D. Mooney (1995), Seismic velocity structure and composition of the continental crust: A global view, *J. Geophys. Res.,* 100, 9761-9788.

Coleman, T. F., and Y. Li (1994), On the convergence of interior-reflective Newton methods for nonlinear minimization subject to bounds, *Math. Progr., 67*, 189-224.

Coleman, T. F., and Y. Li (1996), An interior trust region approach for nonlinear minimization subject to bounds, SIAM J. Optimization, 6(2), 418-445.

Crowhurst, J. C., and J. M. Zaug (2004), Surface acoustic waves in germanium single crystals, *Phys Rev B, 69*, 52301-52304.

Every, A. G., K. Y. Kim, and A. A. Maznev (1998), Surface dynamic response functions of anisotropic solids, *Ultrasonics, 36*, 349–353.

Farnell, G. W. (1970), Properties of elastic surface waves, in *Physical Acoustics*, edited by W. P. Mason and R. N. Thurston, Academic, New York.

Hill R. (1963) Elastic properties of reinforced solids: some theoretical principles. *J Mech Phys. Solids* 11, 357-372

Kroll, H., and P.H. Ribbe (1980), Determinative diagrams for Al,Si order in plagioclases. *Amer. Mineral.*, *65*, 449-457.

Kroll, H., and P.H. Ribbe (1983), Lattice parameters, composition and Al, Si order in alkali feldspars. *Mineral. Soc. Am. Rev. Mineral, 2*, 57-99.

Liebermann, R. C., and A. E. Ringwood (1976), Elastic properties of anorthite and nature of lunar crust, *Earth Planet. Sci. Lett., 31*, 69–74.

Mainprice, D., R. Hielscher, and Schaeben, H. (2011), Calculating anisotropic physical properties from texture data using the MTEX open-source package. From: Prior, D. J., Rutter, E. H. & Tatham, D. J. (eds) Deformation Mechanisms, Rheology and Tectonics: Microstructures, Mechanics and Anisotropy. Geological Society, London, Special Publications, 360, 175–192. DOI: 10.1144/SP360.10

Megaw, H.D. (1970), Structural relationship between coesite and felspar**.** *Acta Cryst. B, 26,* 261-265.

Maznev, A. A., A. Akthakul, and K. A. Nelson (1999), Surface acoustic modes in thin films on anisotropic substrates, *J. Appl. Phys., 86*, 2818–2824.

Mueller, H. J., J. Lauterjung, F. R. Schilling, C. Lathe, and G. Nover (2002), Symmetric and asymmetric interferometric method for ultrasonic compressional and shear wave velocity measurements in piston-cylinder and multi-anvil high-pressure apparatus, *Eur. J. Mineral., 14,* 581–589. doi: 10.1127/0935-1221.

Nye, J. F. (1957), *Physical Properties of Crystals: Their Representation by Tensors and Matrixes*, Oxford, Clarendon Press.

Press, W. H., S. A. Teukolsky, W. T. Vetterling, and B. P. Flannery (2007), *Numerical Recipes: The Art of Scientific Computing*, *Third Edition*, Cambridge University Press, New York.

Ribbe, P.H. (1983), Chemistry, structure, and nomenclature of feldspars. *Mineral. Soc. Am. Rev. Mineral, 2*, 1-19.

Ryzhova, T. V. (1964), Elastic properties of plagioclases, *Akad. SSSR Izv. Ser. Geofiz., 7*, 1049–1051.

Salje, E.K.H. (1985), Thermodynamics of sodium Feldspar. I: order parameter treatment and strain induced coupling effects. *Phys. Chem. Minerals, 12*, 93-98 .

Seront, B., D. Mainprice, and N. I. Christensen (1993), A determination of the 3-dimensional seismic properties of anorthosite—comparison between values calculated from the petrofabric and direct laboratory measurements, *J. Geophys. Res., 98*, 2209–2221.

Simmons, G. (1964), Velocity of shear waves in rocks to 10 kilobars, *J. Geophys. Res., 69*, 1123-1130.

Sochalski-Kolbus, L., R. J. Angel, and F. Nestola (2010), The effect of Al,Si disorder on the bulk moduli of plagioclase feldspars, *Mineralogical Magazine*, **74**, 943-950.

Smith, J. V., W. L. Brown (1988) *Feldspar Minerals I: crystal structures, physical, chemical, and microtextural properties*, Springer Verlage, New York.

Tribaudino M., R. J. Angel, F. Camara, F. Nestola, D. Pasqual, and I. Margiolaki (2010), Thermal expansion of plagioclase feldspars, *Contrib. Min. Petr.,* **160**, 899-908.

Tribaudino, M., M. Bruno, F. Nestola, D. Pasqual, and R. J. Angel (2011), Thermoelastic and thermodynamic properties of plagioclase feldspars from thermal expansion measurements. *Amer. Mineral.*, **96**, 992-1002.

Watt, J. P., G. F. Davies, and R. J. O'Connell (1976), The elastic properties of composite materials, *Rev. Geophys. Space Phys., 14,* 541-563.

Weidner, D. J., and H. R. Carleton (1977), Elasticity of coesite, J. *Geophys. Res., 82*, 1334–1346

Xie, Y., H.-R. Wenk, S. Matthies (2003), Plagioclase preferred orientation by TOF neutron diffraction and SEM-EBSD, *Tectonophysics, 370*, 269–286, doi:10.1016/S0040-1951(03)00191-4.

Table 1: Sample chemistry, unit cell parameters and densities determined from volume and chemical analyses. Data for An_0 are from *Brown et al.* [2006]. Uncertainties in last digit are given in parentheses.

	a: Å	*b*: Å	*c*: Å	α: deg.	β: deg.	γ: deg.	$Å^3$	Density (g/cc)
An_0	8.1366(2)	12.7857(2)	7.1582(3)	94.253(2)	116.605(2)	87.756(2)	663.98(3)	2.623(3)
An_{25}	8.1605(15)	12.8391(6)	7.1288(3)	93.833(13)	116.440(5)	89.124(5)	667.20(13)	2.653(3)
An_{37}	8.16577(9)	12.85623(11)	7.11418(9)	93.622(1)	116.278(1)	89.679(1)	668.123(12)	2.666(3)
An_{48}	8.1744(2)	12.8638(3)	7.1102(2)	93.525(3)	116.236(1)	89.915(3)	669.10(3)	2.683(3)
An_{60}	8.1717(2)	12.8752(2)	14.2074(3)	93.4530(11)	116.078(1)	91.4250(11)	1337.98(5)	2.702(3)
An_{78}	8.1798(3)	12.8761(3)	14.1974(6)	93.423(3)	116.054(3)	90.705(3)	1339.74(8)	2.725(3)
An_{96}	8.1789(3)	12.8717(6)	14.1765(7)	93.194(5)	115.893(3)	91.195(3)	1338.84(10)	2.757(3)

Table 2. Elastic Moduli (GPa units) for Plagioclase Feldspars. Uncertainties in parentheses are 2σ estimates. The first nine entries in each column are moduli that are non-zero for orthorhombic symmetry. The next four (*C_{15}, C_{25}, C_{35}, C_{46}*) are non-zero for monoclinic symmetry and all moduli are non-zero for triclinic symmetry.

GPa	**An_{0}**	**An_{25}**	**An_{37}**	**An_{48}**	**An_{60}**	**An_{78}**	**An_{96}**
"orthorhombic" moduli							
C_{11}	68.3 (0.8)	87.1 (1.3)	96.2 (1.6)	104.6 (1.9)	109.3 (1.7)	120.4 (2.6)	132.2 (3.0)
C_{22}	184.3 (4.9)	174.9 (5.2)	189.4 (4.9)	201.4 (6.6)	185.5 (2.3)	191.6 (6.3)	200.2 (5.4)
C_{33}	180.0 (3.0)	166.1 (4.7)	171.9 (4.5)	172.8 (5.1)	164.1 (1.9)	163.7 (5.0)	163.9 (4.1)
C_{44}	25.0 (0.1)	22.9 (0.2)	23.6 (0.1)	22.9 (0.1)	22.2 (0.1)	23.3 (0.1)	24.6 (0.1)
C_{55}	26.9 (0.1)	29.0 (0.2)	33.1 (0.3)	33.0 (0.3)	33.1 (0.2)	32.8 (0.3)	36.6 (0.2)
C_{66}	33.6 (0.2)	35.0 (0.3)	35.5 (0.3)	35.6 (0.2)	36.8 (0.3)	35.0 (0.5)	36.0 (0.3)
C_{12}	32.2 (1.6)	43.9 (2.0)	46.1 (2.5)	51.5 (2.8)	53.1 (1.1)	56.6 (3.4)	64.0 (3.5)
C_{13}	30.4 (1.5)	35.4 (1.9)	38.4 (2.2)	43.9 (2.4)	42.1 (2.1)	49.9 (2.9)	55.3 (2.8)
C_{23}	5.0 (2.6)	18.0 (3.7)	15.4 (4.0)	14.5 (4.5)	21.9 (2.8)	26.3 (4.5)	31.9 (3.7)
remaining off-diagonal moduli							
C_{15}	-2.3 (0.3)	-0.4 (0.4)	-0.2 (0.4)	0.1 (0.5)	1.2 (0.4)	3.2 (0.6)	5.1 (0.6)
C_{25}	-7.8 (0.7)	-2.9 (0.8)	-5.1 (1.1)	-4.8 (1.2)	0.7 (0.8)	5.4 (1.0)	3.5 (0.9)
C_{35}	7.5 (0.6)	4.6 (0.8)	7.2 (1.1)	6.9 (1.0)	2.5 (0.8)	1.7 (0.9)	0.5 (0.9)
C_{46}	-7.2 (0.1)	-5.2 (0.2)	-4.8 (0.2)	-3.8 (0.2)	1.4 (0.1)	0.9 (0.2)	-2.2 (0.1)
C_{14}	4.9 (0.2)	6.1 (0.3)	5.9 (0.3)	6.5 (0.4)	7.6 (0.3)	9.0 (0.5)	9.5 (0.5)
C_{16}	-0.9 (0.3)	-0.6 (0.4)	-0.4 (0.5)	-0.8 (0.5)	-7.7 (0.5)	-3.0 (0.6)	-10.8 (0.7)
C_{24}	-4.4 (0.6)	-5.9 (0.6)	-7.0 (0.6)	-2.4 (0.6)	-2.9 (0.5)	2.1 (0.9)	7.5 (0.6)
C_{26}	-6.4 (0.9)	-6.5 (0.9)	-6.8 (1.2)	-9.9 (1.2)	-6.8 (1.1)	-9.9 (1.3)	-7.2 (1.3)
C_{34}	-9.2 (0.4)	-2.9 (0.5)	2.2 (0.7)	-0.4 (0.5)	0.2 (0.5)	1.7 (0.9)	6.6 (0.6)
C_{36}	-9.4 (0.6)	-10.7 (0.9)	-9.8 (0.9)	-5.7 (1.0)	0.7 (0.8)	-8.1 (1.1)	1.6 (1.0)
C_{45}	-2.4 (0.1)	-1.3 (0.1)	-1.1 (0.2)	-1.0 (0.2)	0.2 (0.1)	0.8 (0.1)	3.0 (0.1)
C_{56}	0.6 (0.1)	0.8 (0.2)	1.4 (0.2)	2.1 (0.3)	2.8 (0.2)	4.5 (0.3)	5.2 (0.2)

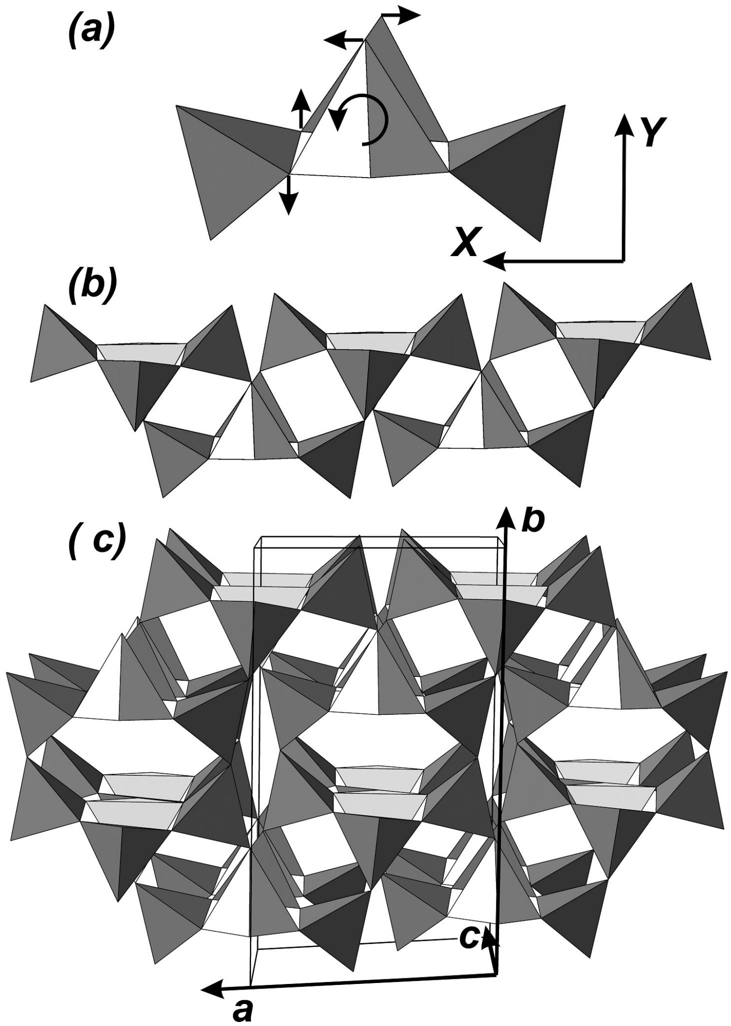

Figure 1: A polyhedral representation of the components of the alumino-silicate framework of plagioclase feldspars, as illustrated by the structure of albite. Each tetrahedron represents a SiO_4 or AlO_4 unit with an O atom at each tetrahedral corner. All oxygen atoms are shared between two tetrahedra. The framework is built from 4-rings of tetrahedra (a) which are free to rotate around their inner edges. The rings can also shear, and exhibit a torsional tilt with atom motions indicated by the arrows. The rings are combined to form the crankshaft chain (b). Changes in the torsional tilt of the rings results in large changes in length of this chain. The chains are assembled to form the entire 3-dimensional framework (c). The directions of both the crystallographic axes and the Cartesian axes X and Y are indicated.

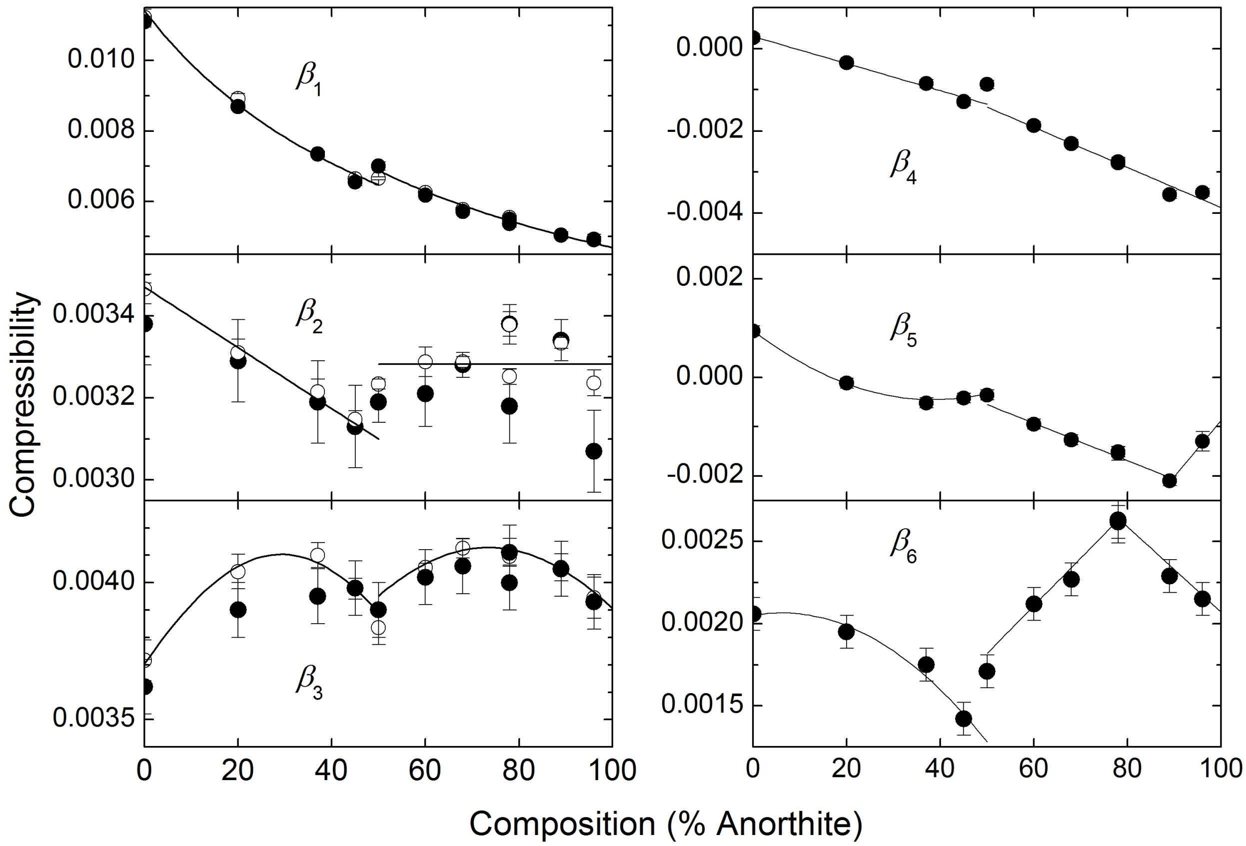

Figure 2 Variation of room-pressure compressibilities (GPa^{-1}) with composition, as determined by high-pressure single-crystal X-ray diffraction measurements of the unit-cell parameter variation with pressure as determined in this work and by *Angel* [2004]. Closed symbols represent fits to incremental strain data. Open symbols are from fits of Birch-Murngahan equations of state to the variations with pressure of the cubes of the unit-cell dimensions corresponding to the X, Y, and Z Cartesian axial directions. Lines are polynomial fits through the data.

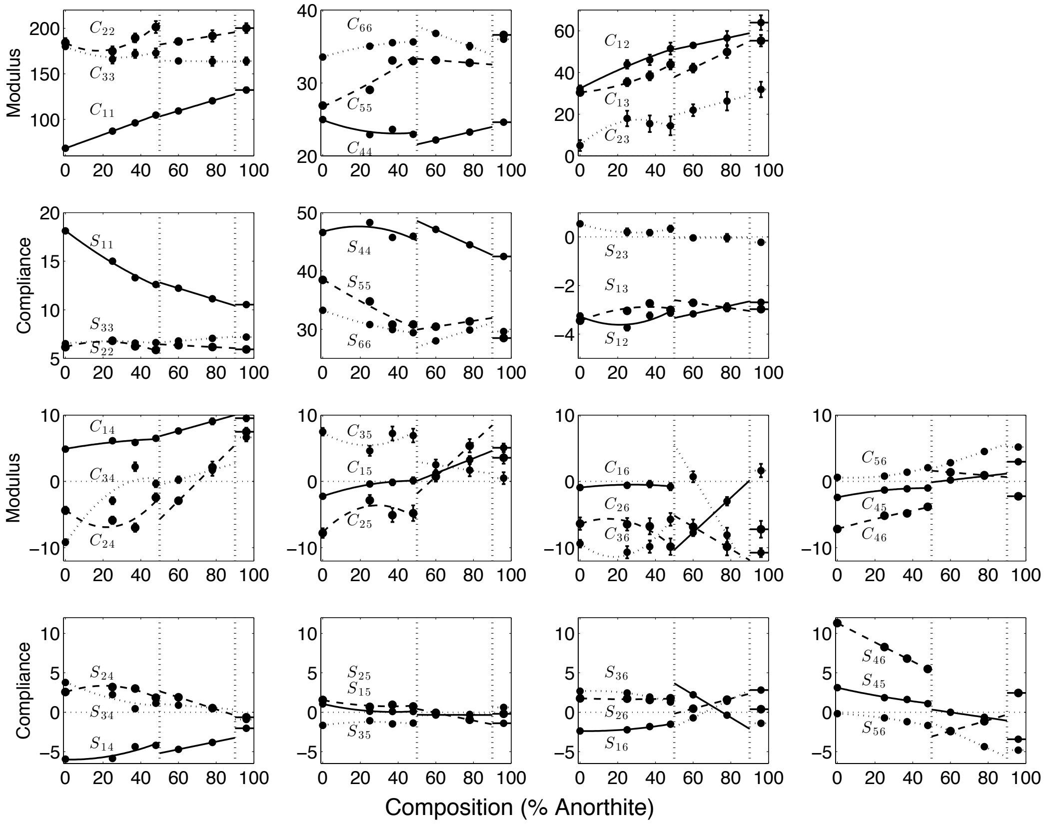

Figure 3. Elastic moduli (GPa) and compliances (TPa^{-1}) for plagioclase series feldspars. Top two rows: the "orthorhombic" moduli/compliances versus composition. Bottom two rows: The remaining (off-diagonal) moduli/compliances versus composition. Vertical dashed lines at An_{50} and An_{90} show boundaries between $C\bar{1}$, $I\bar{1}$, and $P\bar{1}$ phases. Elastic matrix elements are labeled in each panel and a (solid-dashed-dotted) curve follows each element across the compositional space. Error bars (when larger than symbol size) are 2σ estimates.

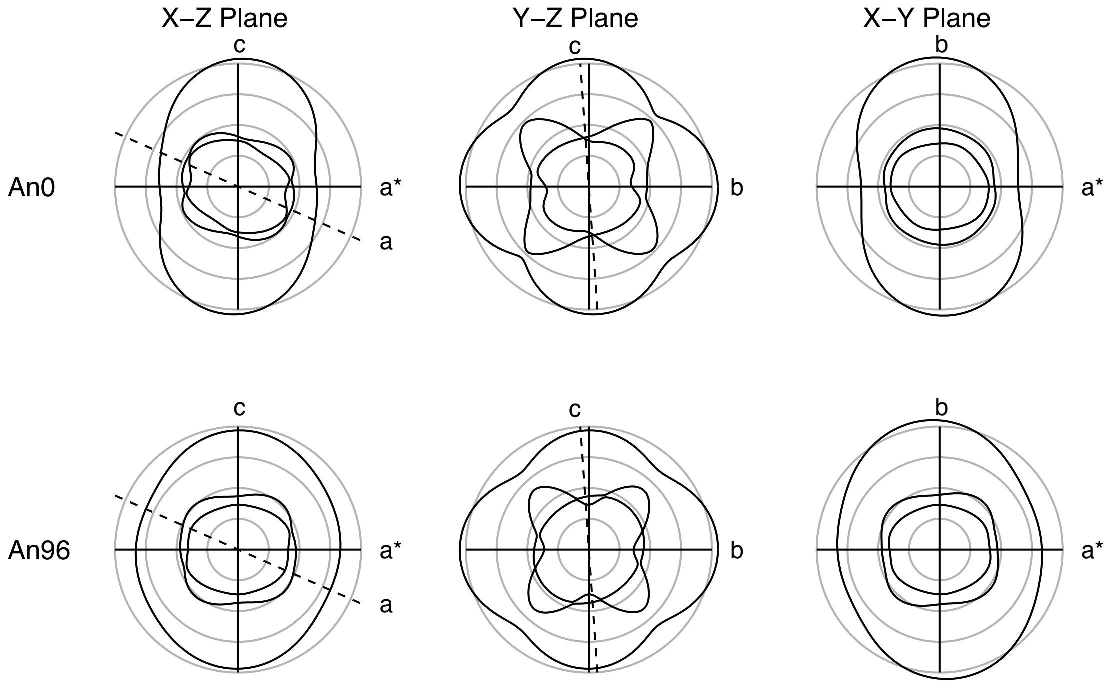

Figure 4. Elastic wave velocities in three orthogonal planes for (near) endmember plagioclase compositions. Grey circles are iso-velocity lines at 2, 4, 6, and 8 km/s. Crystallographic axes (or their projections on the plane) are indicated. Velocities are plotted in radial coordinates using solid lines. The inner curves are the quasi-shear branches and the outer curve in each figure is the quasi-compressional branch.

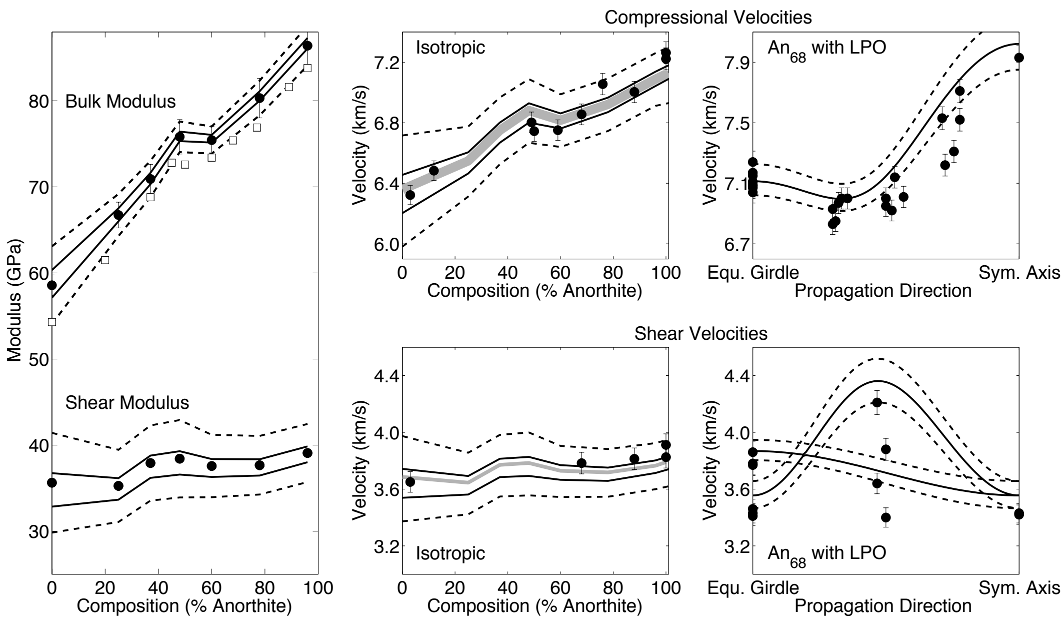

Figure 5. Orientational averaged properties for plagioclase feldspars. Left side: Isotropic elastic moduli as a function of plagioclase composition. Hill average points are plotted as filled circles (uncertainties are 2σ, those for the shear modulus are within symbol size). Voigt (upper) and Reuss (lower) bounds are plotted with dashed lines. Hashin-Shtrikman upper and lower bounds are plotted as solid lines connecting the points. Open squares are the bulk moduli determined by single-crystal high-pressure X-ray diffraction measurements. Middle: Isotropic body-wave velocities for plagioclase as a function of composition. Symbols: Literature values for compression and shear wave velocities measured at a nominal pressure of 1 GPa and corrected to one bar (Auxiliary Data Table S4). Dashed lines are Voigt and Reuss bounds based on the current data. Solid lines are the Hashin-Shtrikman bounds, The grey line is the Hill average with propagated uncertainties indicated by the line width. Right: Compressional and shear wave velocities for an anorthosite (90% An_{68} 10% Fo_{90}) with LPO. Circles- data of *Seront et al,* [1993] at 0.8 GPa projected onto transverse anisotropy coordinates. Dashed lines are Voigt and Reuss bounds, and the solid line is the Hill average using a statistical ensemble of orientations for An_{68} crystals that has a variance of 25° in alignment of *b*-axes. 10% isotropic olivine is included in the average. All calculated compressional velocities are shifted up by 0.08 km/s to account for the pressure dependence from measured one-bar elastic moduli. No pressure correction is applied to the shear wave velocities.